INTERNATIONAL JOURNAL FOR NUMERICAL METHODS IN ENGINEERING

Int. J. Numer. Meth. Engng 2009; **00**:1–36 *Prepared using* nmeauth.cls *[Version: 2002/09/18 v2.02]*

Fracture in magnetoelectroelastic materials using the extended finite element method

R. Rojas-Díaz[1], N. Sukumar[2], A. Sáez[1,*]and F. García-Sánchez[3]

[1] *Departamento de Mecánica de los Medios Continuos, Escuela Técnica Superior de Ingenieros, Universidad de Sevilla, 41092-Sevilla, Spain.*

[2] *Department of Civil and Environmental Engineering, University of California, Davis, CA 95616, USA.*

[3] *Departamento de Ingeniera Civil, de Materiales y Fabricación, ETS de Ingenieros Industriales, 29013 Málaga*

SUMMARY

Static fracture analyses in two-dimensional linear magnetoelectroelastic solids is studied by means of the extended finite element method (X-FEM). In the X-FEM, crack modeling is facilitated by adding a discontinuous function and the crack-tip asymptotic functions to the standard finite element approximation using the framework of partition of unity. In this study, media possessing fully coupled piezoelectric, piezomagnetic and magnetoelectric effects are considered. New enrichment functions for cracks in transversely isotropic magnetoelectroelastic materials are derived, and the computation of fracture parameters using the domain form of the contour interaction integral is presented. The convergence rates in energy for topological and geometric enrichments are studied. Excellent accuracy

*Correspondence to: A. Sáez, Departamento de Mecánica de los Medios Continuos, Escuela Superior de Ingenieros, Universidad de Sevilla, Camino de los Descubrimientos S/N, 41092-Sevilla, Spain. E-mail: andres@us.es

Received 00

Revised 00

Accepted 00

of the proposed formulation is demonstrated on benchmark crack problems through comparisons with both analytical solutions and numerical results obtained by the dual boundary element method.

KEY WORDS: partition of unity enrichment, X-FEM, magnetoelectroelasticity, interaction integral

1. INTRODUCTION

The use of magnetoelectroelastic (MEE) materials is receiving increasing attention due to the inherent coupling among mechanical, electric and magnetic fields. Such coupling provides new technological possibilities in novel multifunctional devices, such as electromagnetic transducers, actuators, and sensors. Natural MEE single-phase materials are rare, and their electromagnetic coupling is either relatively weak or it occurs at low temperatures for practical applications. In contrast, composites that combine both piezomagnetic and piezoelectric phases typically show much larger electromagnetic response above room temperature. Such electromagnetic coupling is a new product property of the resulting composite, since it is absent in both the piezoelectric and piezomagnetic phases when considered alone. A review on the current status of MEE composites can be found in the work by Nan et al. [1].

Fracture mechanics of this class of materials is relevant to predict the structural integrity and in-service working conditions of MEE devices. However, as compared to the anisotropic or piezoelectric cases, relatively limited work has been done when it comes to analyze fracture phenomena in magnetoelectroelastic materials. Related to static fracture, Gao et al. [2–5] analyzed some basic problems analytically, whereas in the works by Sih et al. [6–8] and Song and Sih [9] the influence of both electromagnetic fields and the volume fraction of

the magnetoelectroelastic composite on crack initiation and growth are analysed. Wang and Mai [10, 11] derived the expressions for the magnetoelectroelastic asymptotic fields, as well as path-independent integrals. Using such path independent integrals, fracture behaviour of magnetoelectroelastic solids was analyzed by Tian and Rajapakse [12]. All these studies present analytical procedures that are limited to problems with relatively simple geometries and loading conditions.

Several numerical methods have been proposed to solve static fracture mechanics problems in magnetoelectroelastic solids. A dual boundary element (BE) formulation was presented by García-Sánchez et al. [13], whereas Sladek et al. [14] proposed a meshless local Petrov-Galerkin approach. In contrast, limited work has been done so far to model MEE structures using finite element methods (FEM). Buchanan [15] applied FEM to obtain the multiphase material properties. Garcia Lage et al. [16] developed a partial mixed layerwise finite element model for the static and free vibration analysis of MEE laminated plate structures. Bhangale and Ganesan [17] presented a semi-analytical FEM for the static analysis of functionally graded, anisotropic and linear MEE plates. This work was further extended by Rajesh et al. [18] to the case of free vibrations of plates and by Annigeri et al. [19] to the problem of free vibrations of clamped-clamped cylindrical shells. More recently, Daga et al. [20] analyzed the sensory response of MEE materials bonded on the top surface of a mild steel beam under transient mechanical loading using finite elements and Simoes Moita et al. [21] proposed a FE model based on third-order shear deformation theory, for static and free vibration analysis of plate structures integrating piezoelectric/piezomagnetic layers.

Related to fracture applications, different crack-face boundary conditions were analysed by Wang and Mai [22] using a classical finite element approach, in which the mesh boundaries

must align with the crack path. Additionally, mesh refinement or singular elements such as quarter-point elements are also necessary near the crack-tip to capture the stress singularity. To circumvent these difficulties, the extended finite element method (X-FEM) is a powerful alternative in computational fracture. In the X-FEM, the crack discontinuity is represented by enriching the classical finite element approximation by discontinuous and near-tip asymptotic functions via the framework of partition of unity. The X-FEM has been successfully applied to solve crack problems by Moës et al. [23] in isotropic media, Sukumar et al. [24] in bimaterials, Asadpoure and Mohammadi [25] in orthotropic materials, and Béchet et al. [26] in piezoelectric media. It is well-established in the literature (for example, see Fries and Belytscho [27]) that the X-FEM with near-tip enrichment is more accurate and efficient than conventional FEM with no enrichment.

In this paper, we present extended finite element analyses for fracture in two-dimensional in-plane transversely isotropic MEE materials. The governing equations are stated in Section 2, and the crack-tip asymptotic fields (used to design the enrichment functions) in MEE materials are provided in Section 3. The extended finite element formulation is presented in Section 4, and new crack-tip enrichment functions for MEE materials are derived in Section 5. The computation of fracture parameters using the domain form of the contour interaction integral is described in Section 6, and supportive numerical fracture results for the extended stress intensity factors are presented in Section 7 to validate the formulation. We close with the main findings from this study in Section 8.

2. GOVERNING EQUATIONS FOR LINEAR MAGNETOELECTROELASTICITY

For a composite material in which both piezoelectric and elastomagnetic phases coexist, the interaction among the electric, magnetic and mechanical fields leads to the following constitutive equations for the resulting linear MEE solid [28]:

$$\sigma_{ij} = c_{ijkl}\varepsilon_{kl} - e_{lij}E_l - h_{lij}H_l \tag{1a}$$

$$D_i = e_{ikl}\varepsilon_{kl} + \epsilon_{il}E_l + \beta_{il}H_l \tag{1b}$$

$$B_i = h_{ikl}\varepsilon_{kl} + \beta_{il}E_l + \gamma_{il}H_l \tag{1c}$$

where σ_{ij} are the components of the Cauchy stress tensor, D_i are the electric displacements, and B_i are the magnetic inductions. In addition, ε_{ij} are the components of the small-strain elastic tensor, and E_i and H_i are the electric and magnetic fields, respectively. In (1), C_{ijkl}, ϵ_{il} and γ_{il} are the elastic stiffness tensor, the dielectric permittivities and the magnetic permeabilities, respectively, whereas e_{lij}, h_{lij} and β_{il} are the piezoelectric, piezomagnetic and electromagnetic coupling coefficients, respectively.

Small displacement gradients are assumed, so that the linearized strain-displacement relations hold. The electric and the magnetic fields are the gradient of the electric potential ϕ and the magnetic potential φ, respectively

$$\varepsilon_{ij} = \frac{1}{2}(u_{i,j} + u_{j,i}) \tag{2a}$$

$$E_i = -\phi_{,i} \tag{2b}$$

$$H_i = -\varphi_{,i} \tag{2c}$$

where u_i are the elastic displacement components. The summation rule on repeated indices is implied unless otherwise stated and a comma stands for partial differentiation.

The equilibrium equations for static loading are given by

$$\sigma_{ij,j} = -f_i^{mech} \tag{3a}$$

$$D_{i,i} = f^e \tag{3b}$$

$$B_{i,i} = f^m \tag{3c}$$

where f_i^{mech} are the body forces and f^e and f^m are the electric charge density and the electric current density, respectively.

Following the notation first introduced by Barnett and Lothe [29] for piezoelectricity, a generalized displacement vector is defined by extending the elastic displacement vector with the electric and magnetic potentials as

$$u_I = \begin{cases} u_i & \text{I=1,2,3} \\ \phi & \text{I=4} \\ \varphi & \text{I=5} \end{cases} \tag{4}$$

and a generalized stress tensor is defined by the extension of the elastic stresses with the electric displacements and the magnetic inductions as

$$\sigma_{iJ} = \begin{cases} \sigma_{ij} & \text{J=1,2,3} \\ D_i & \text{J=4} \\ B_i & \text{J=5} \end{cases} \tag{5}$$

so that the linear MEE problem can be formulated in an elastic-like fashion. The constitutive equations (1) may be recast is a more compact form to yield

$$\sigma_{iJ} = c_{iJKl} u_{K,l} \tag{6}$$

where the lowercase subscripts (elastic) vary from 1 to 3, whereas the uppercase ones (extended) vary from 1 to 5. The material properties have been grouped together into a

generalized elasticity tensor defined as

$$c_{iJKl} = \begin{cases} c_{ijkl} & J,K = 1,2,3 \\ e_{lij} & J = 1,2,3;\ K = 4 \\ h_{lij} & J = 1,2,3;\ K = 5 \\ e_{ikl} & J = 4;\ K = 1,2,3 \\ -\epsilon_{il} & J,K = 4 \\ -\beta_{il} & J = 4;\ K = 5 \\ h_{ikl} & J = 5;\ K = 1,2,3 \\ -\beta_{il} & J = 5;\ K = 4 \\ -\gamma_{il} & J,K = 5 \end{cases} \tag{7}$$

3. GENERALIZED DISPLACEMENT FIELDS AROUND A CRACK IN A MAGNETOELECTROELASTIC SOLID

The asymptotic terms of the generalized displacement fields in the vicinity of a crack tip must be included in the extended formulation of the finite element to describe the crack-discontinuity. To this end, we next derive such asymptotic crack-tip fields in the vicinity of a crack in a MEE material, based on Laurent's series expansions.

In this wor,k we consider transversely isotropic MEE media under generalized plane strain

conditions. In such a case, the constitutive relations (6) may be further reduced to [30]

$$\begin{Bmatrix} \varepsilon_{11} \\ \varepsilon_{22} \\ 2\varepsilon_{12} \\ E_1 \\ E_2 \\ H_1 \\ H_2 \end{Bmatrix} = \begin{pmatrix} a_{11} & a_{12} & 0 & 0 & b_{21} & 0 & d_{21} \\ a_{12} & a_{22} & 0 & 0 & b_{22} & 0 & d_{22} \\ 0 & 0 & a_{33} & b_{13} & 0 & d_{13} & 0 \\ 0 & 0 & -b_{13} & \delta_{11} & 0 & \Delta_{11} & 0 \\ -b_{21} & -b_{22} & 0 & 0 & \delta_{22} & 0 & \Delta_{22} \\ 0 & 0 & -d_{13} & \Delta_{11} & 0 & \zeta_{11} & 0 \\ -d_{21} & -d_{22} & 0 & 0 & \Delta_{22} & 0 & \zeta_{22} \end{pmatrix} \begin{Bmatrix} \sigma_{11} \\ \sigma_{22} \\ \sigma_{12} \\ D_1 \\ D_2 \\ B_1 \\ B_2 \end{Bmatrix} \tag{8}$$

where the terms in the matrix are listed in appendix A.

The equilibrium equations in the absence of generalized body forces are

$$\frac{\partial \sigma_{11}}{\partial x_1} + \frac{\partial \sigma_{12}}{\partial x_2} = 0, \quad \frac{\partial \sigma_{12}}{\partial x_1} + \frac{\partial \sigma_{22}}{\partial x_2} = 0 \tag{9a}$$

$$\frac{\partial D_1}{\partial x_1} + \frac{\partial D_2}{\partial x_2} = 0 \tag{9b}$$

$$\frac{\partial B_1}{\partial x_1} + \frac{\partial B_2}{\partial x_2} = 0 \tag{9c}$$

and the compatibility conditions are

$$\frac{\partial^2 \varepsilon_{11}}{\partial x_2^2} + \frac{\partial^2 \varepsilon_{22}}{\partial x_1^2} = 2\frac{\partial^2 \varepsilon_{12}}{\partial x_1 \partial x_2} \tag{10a}$$

$$\frac{\partial E_1}{\partial x_2} - \frac{\partial E_2}{\partial x_1} = 0 \tag{10b}$$

$$\frac{\partial H_1}{\partial x_2} - \frac{\partial H_2}{\partial x_1} = 0 \tag{10c}$$

Let us now introduce the potential functions U, χ and ϑ defined by

$$\sigma_{11} = U(x_1, x_2)_{,22}, \quad \sigma_{22} = U(x_1, x_2)_{,11}, \quad \sigma_{12} = -U(x_1, x_2)_{,12} \tag{11a}$$

$$D_1 = \chi(x_1, x_2)_{,2}, \quad D_2 = -\chi(x_1, x_2)_{,1} \tag{11b}$$

$$B_1 = \vartheta(x_1, x2)_{,2}, \quad B_2 = -\vartheta(x_1, x2)_{,1} \tag{11c}$$

The equilibrium equations (9) are automatically satisfied because of the definitions in (11). Substituting (8) into (10) and expressing the stresses, the electric displacements and the magnetic inductions by the potentials in (11) leads to

$$\begin{aligned} &a_{11}U_{,2222} + a_{22}U_{,1111} + (2a_{12} + a_{33})U_{,1122} - (b_{21} + b_{13})\chi_{,122} \\ &-b_{22}\chi_{,111} - (d_{21} + d_{13})\vartheta_{,122} - d_{22}\vartheta_{,111} = 0 \end{aligned} \tag{12a}$$

$$(b_{21} + b_{13})U_{,122} + b_{22}U_{,111} + \delta_{11}\chi_{,22} + \delta_{22}\chi_{,11} + \Delta_{11}\vartheta_{,22} + \Delta_{22}\vartheta_{,11} = 0 \tag{12b}$$

$$(d_{21} + d_{13})U_{,122} + d_{22}U_{,111} + \Delta_{11}\chi_{,22} + \Delta_{22}\chi_{,11} + \zeta_{11}\vartheta_{,22} + \zeta_{22}\vartheta_{,11} = 0 \tag{12c}$$

so that on defining the following operators

$$L_4 = a_{22}\frac{\partial^4}{\partial x_1^4} + a_{11}\frac{\partial^4}{\partial x_2^4} + (2a_{11} + a_{33})\frac{\partial^4}{\partial x_1^2 \partial x_2^2} \tag{13a}$$

$$L_3 = b_{22}\frac{\partial^3}{\partial x_1^3} + (b_{21} + b_{13})\frac{\partial^3}{\partial x_1 \partial x_2^2} \tag{13b}$$

$$M_3 = d_{22}\frac{\partial^3}{\partial x_1^3} + (d_{21} + d_{13})\frac{\partial^3}{\partial x_1 \partial x_2^2} \tag{13c}$$

$$L_2 = \delta_{22}\frac{\partial^2}{\partial x_1^2} + \delta_{11}\frac{\partial^2}{\partial x_2^2} \tag{13d}$$

$$M_2 = \Delta_{22}\frac{\partial^2}{\partial x_1^2} + \Delta_{11}\frac{\partial^2}{\partial x_2^2} \tag{13e}$$

$$P_2 = \zeta_{22}\frac{\partial^2}{\partial x_1^2} + \zeta_{11}\frac{\partial^2}{\partial x_2^2} \tag{13f}$$

the compatibility equations can be reduced to the following partial differential equation of eighth order for $U(x_1, x_2)$ (see Reference [31] for details)

$$[L_4(L_2P_2 - M_2^2) + L_3(L_3P_2 - 2M_3M_2) + L_2M_3^2]U = 0 \tag{14}$$

whose solution can be derived in the form

$$U(x_1, x_2) = U(x_1 + \mu x_2) \quad \text{with} \quad \mu = \mathrm{Re}(\mu) + i\mathrm{Im}(\mu) \tag{15}$$

Substitution of (15) into (14) leads to the following eighth order characteristic equation for

the complex roots μ_i

$$\begin{aligned}&[a_{11}\mu^4+(2a_{12}+a_{33})\mu^2+a_{22}][(\Delta_{11}\mu^2+\Delta_{22})^2-(\delta_{11}\mu^2+\delta_{22})(\zeta_{11}\mu^2+\zeta_{22})]\\&-[(b_{21}+b_{13})\mu^2+b_{22}]^2(\zeta_{11}\mu^2+\zeta_{22})-[(d_{21}+d_{13})\mu^2+d_{22}]^2(\delta_{11}\mu^2+\delta_{22})\\&+2[(b_{21}+b_{13})\mu^2+b_{22}][(d_{21}+d_{13})\mu^2+d_{22}](\Delta_{11}\mu^2+\Delta_{22})=0\end{aligned} \tag{16}$$

The general solution for $U(x_1,x_2)$ can be constructed by means of the eight roots μ_i, which are actually four conjugate complex pairs, as

$$U(x_1,x_2)=\sum_{i=1}^{8}U_i(x_1+\mu_i x_2) \tag{17}$$

The potentials $\chi(x_1,x_2)$ and $\vartheta(x_1,x_2)$ can be derived from $U(x_1,x_2)$ by combining equations (8), (10) and (11) (see References [31] and [26] for details), so that all the magnetoelectromechanical variables can be obtained by means of the potential $U(x_1,x_2)$.

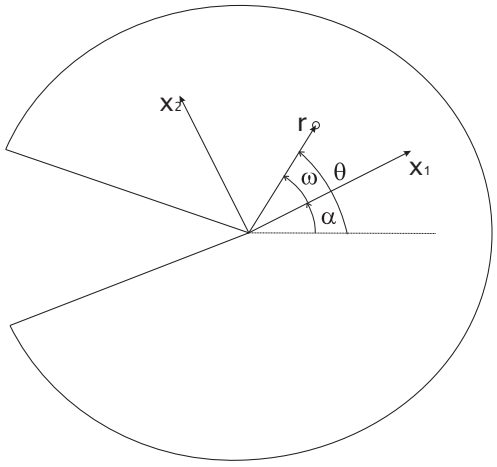

Figure 1. Definition of the material axes around the crack tip

The displacement solution in the vicinity of a crack is now derived in an unbounded plane domain (Figure 1). Let x_2 be the polarization direction and α the angle between the crack line and the material coordinate system (x_1,x_2) with origin at the crack tip. Extending to

the MEE case the procedure presented in Reference [26] for piezoelectrics, the potential U in equation (17) is expanded in a Laurent-like series:

$$U(x_1, x_2) = \sum_k \sum_{i=1}^{8} d_i(\lambda_k)(x_1 + \mu_i x_2)^{\lambda_k + 2} \tag{18}$$

where $d_i(\lambda_k)$ are complex free coefficients of the series expansion to be determined and λ_k are generally complex and represent the number of roots of the solvability equation for the crack faces boundary conditions considered. In this paper, we will focus on traction-free cracks with electric and magnetic impermeable crack face boundary conditions, i.e., with zero normal electric displacement and magnetic induction on the crack faces [22].

On considering a polar coordinate system with the origin at the crack tip, the real potential $U(r, \theta)$ in (18) can be rewritten as

$$U(r,\theta) = \sum_{i=1}^{4} d_i(\lambda) r(\cos(\theta - \alpha) + \mu_i \sin(\theta - \alpha))^{\lambda+2} + \sum_{i=1}^{4} \overline{d_i(\lambda)} r(\cos(\theta - \alpha) + \overline{\mu_i} \sin(\theta - \alpha))^{\lambda+2}$$

where λ is one of the λ_k in (18) and it is assumed to be real.

The real representation of each term in (18) for each μ_i leads to expressions of the form

$$e_i p^{\lambda+2} \cos\left[(\lambda + 2)(\kappa + \frac{\pi}{2})\right] + f_i p^{\lambda+2} \sin\left[(\lambda + 2)(\kappa + \frac{\pi}{2})\right] \tag{19a}$$

with

$$p = r\sqrt{(|\mu_K|^2 - 1)(\sin\omega)^2 + \mathrm{Re}(\mu_i)(\sin 2\omega)} \tag{19b}$$

$$\kappa = \arctan \frac{1 + \mathrm{Re}(\mu_i)\tan(\omega)}{|\mathrm{Im}(\mu_i)|\tan(\omega)} \tag{19c}$$

$$d_i(\lambda) = e_i(\lambda) + i f_i(\lambda) \tag{19d}$$

$$\omega = \theta - \alpha \tag{19e}$$

where e_i and f_i are eight unknown coefficients. As pointed out by Béchet et al. [26] for piezoelectricity, an infinite number of λ_k may be obtained as

$$\lambda_1 = -1/2, \quad \lambda_2 = 0, \quad \lambda_3 = 1/2, \quad \lambda_4 = 1 \dots \tag{20}$$

for impermeable crack-face boundary conditions. The first root $\lambda_1 = -1/2$ generates four independent eigenvectors (and their respective conjugate complex pairs) so that four independent singular eigenfunctions, which incorporate the classical $1/\sqrt{r}$ crack tip singularity, can be constructed. These independent eigenfunctions can be used for obtaining the enrichment functions for the X-FEM.

It is noteworthy to point that these enrichment functions depend on the angle $\omega = \theta - \alpha$ and hence, the enrichment functions can be calculated for every poling direction with respect to the crack line.

4. EXTENDED FINITE ELEMENT FORMULATION

The extended finite element method [23, 32] is a technique to simulate crack discontinuities without the need for the crack to conform to the finite element mesh. To this end, additional (enrichment) functions are added to the classical finite element approximation through the framework of partition of unity [33]. The crack interior is represented by a discontinuous (Heaviside) function and the crack-tip is modeled by the asymptotic crack-tip functions.

4.1. Crack modeling and selection of enriched nodes

Consider a crack $\Gamma_c = \Gamma_c^- \cup \Gamma_c^+$ located inside a domain $\Omega \subset \mathbf{R}^2$ with boundary Γ. The domain is discretized by finite elements, and let $\mathcal{N}$ denote the nodal set. Generalized displacements are prescribed on Γ_u, whereas generalized tractions are imposed on Γ_t, so that $\Gamma = \Gamma_u \cup \Gamma_t$

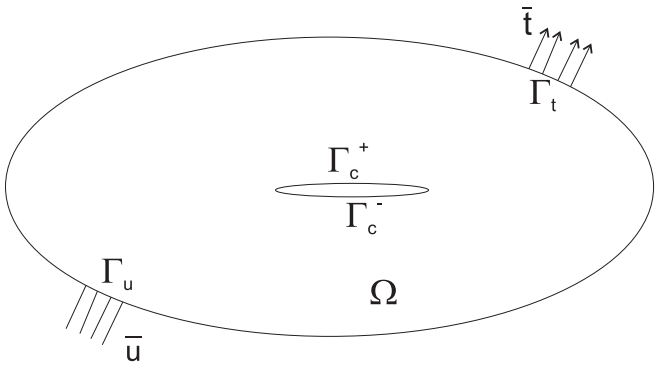

Figure 2. Boundary value problem with an internal crack.

(Figure 2). The displacement approximation (trial function) in the X-FEM is written as [23]

$$\mathbf{u}^h(\mathbf{x}) = \sum_{i\in\mathcal{N}} N_i(\mathbf{x})\mathbf{u}_i + \sum_{j\in\mathcal{N}^{\mathcal{H}}} N_j(\mathbf{x})H(\mathbf{x})\boldsymbol{a}_j + \sum_{k\in\mathcal{N}^{C\mathcal{T}}} N_k(\mathbf{x})\sum_{\alpha} F_\alpha(\mathbf{x})\boldsymbol{b}_k^\alpha \tag{21}$$

where N_i is the standard finite element shape function associated with node i, $\mathbf{u}_i$ is the vector of nodal degrees of freedom defined in classical finite elements, and $\mathbf{a}_j$ and $\mathbf{b}_k^\alpha$ are the added set of degrees of freedom in the elements containing the crack. $H(\mathbf{x})$ is the generalized Heaviside function, which enables the modeling of a crack that fully cuts a finite element, and F_α are the crack-tip enrichment functions. In a MEE solid, the variables that appear in (21) are defined in an extended way, so $\mathbf{u}_i$ and $\mathbf{a}_j$ are 4-component vectors and $\mathbf{b}_k^\alpha$ is a 32-component vector, since four nodal variables (u_1, u_2, ϕ, φ) and eight enrichment functions are involved. In isotropic elastic materials $\mathbf{b}_k^\alpha$ is an 8-component vector, since only two nodal variables (u_1, u_2) and four enrichment functions are needed to describe all the possible deformation states in the vicinity of the crack-tip [23].

In a finite element mesh (Figure 3), the nodes that are enriched with the Heaviside function (set $\mathcal{N}^H$) are marked with a filled circle and they belong to elements fully cut by the crack, whereas the nodes that are enriched with crack-tip enrichment functions (set $\mathcal{N}^{CT}$) are marked

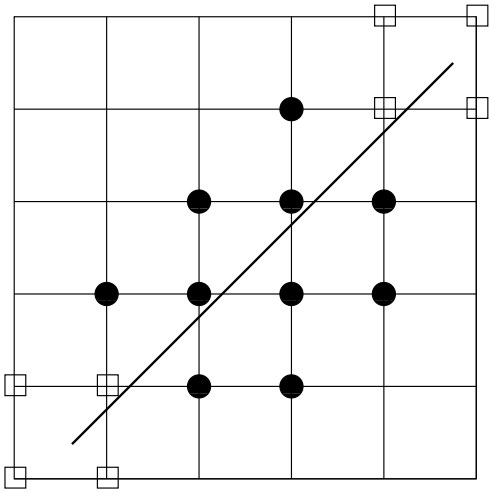

Figure 3. Node selection for topological enrichment.

with a square and they belong to elements that contain the crack tip.

4.2. Weak formulation and discrete equations

Let $\widetilde{\mathbf{u}}$ be the mechanical displacement and $\widetilde{\boldsymbol{\sigma}}$ the mechanical stress tensor, whereas $\mathbf{u}$ and $\boldsymbol{\sigma}$ are, respectively, the extended displacement vector and the extended stress tensor. The weak form (principle of virtual work) for a continuous problem in a MEE solid is given by

$$\int_\Omega \widetilde{\boldsymbol{\sigma}} : \delta\widetilde{\boldsymbol{\varepsilon}}\, d\Omega - \int_\Omega \mathbf{D} : \delta\mathbf{E}\, d\Omega - \int_\Omega \mathbf{B} : \delta\mathbf{H}\, d\Omega = \int_{\Gamma_t} \overline{\mathbf{t}}^{mech} \cdot \delta\widetilde{\mathbf{u}} d\Gamma - \int_{\Gamma_t} \overline{\mathbf{t}}^{\mathbf{e}} \cdot \delta\boldsymbol{\phi}\, d\Gamma - \int_{\Gamma_t} \overline{\mathbf{t}}^{\mathbf{m}} \cdot \delta\boldsymbol{\varphi}\, d\Gamma + \int_\Omega \mathbf{f}^{mech} \cdot \delta\widetilde{\mathbf{u}}\, d\Omega - \int_\Omega \mathbf{f}^{e} \cdot \delta\boldsymbol{\phi}\, d\Omega - \int_\Omega \mathbf{f}^{m} \cdot \delta\boldsymbol{\varphi}\, d\Omega. \tag{22}$$

Since the MEE problem can be expressed in an elastic-like way, (22) can be rewritten as

$$\int_\Omega \boldsymbol{\sigma} : \delta\boldsymbol{\varepsilon}\, d\Omega = \int_{\Gamma_t} \overline{\mathbf{t}} \cdot \delta\mathbf{u} + d\Gamma + \int_\Omega \mathbf{f} \cdot \delta\mathbf{u}\, d\Omega \tag{23}$$

by using the extended variables notation introduced in Section 2. In (23), $\overline{\mathbf{t}}$ are the prescribed extended tractions and $\mathbf{f}$ is the extended volume forces vector.

After the appropriate discretizations of the governing equations, the following MEE finite element equations can be derived:

$$\mathbf{k}_{\widetilde{u}\widetilde{u}}\widetilde{\mathbf{u}} + \mathbf{k}_{\widetilde{u}\phi}\boldsymbol{\phi} + \mathbf{k}_{\widetilde{u}\varphi}\boldsymbol{\varphi} = f^{mech} \tag{24a}$$

$$\mathbf{k}_{\phi\widetilde{u}}\widetilde{\mathbf{u}} - \mathbf{k}_{\phi\phi}\boldsymbol{\phi} - \mathbf{k}_{\phi\varphi}\boldsymbol{\varphi} = f^{e} \tag{24b}$$

$$\mathbf{k}_{\varphi\widetilde{u}}\widetilde{\mathbf{u}} - \mathbf{k}_{\varphi\phi}\boldsymbol{\phi} - \mathbf{k}_{\varphi\varphi}\boldsymbol{\varphi} = f^{m} \tag{24c}$$

which can be grouped together to yield

$$\mathbf{K} = \bigwedge_{e} \mathbf{k}_e, \quad \mathbf{f} = \bigwedge_{e} \mathbf{f}_e \tag{25a}$$

as the global stiffness matrix and force vector, respectively, and

$$\mathbf{k}_e\mathbf{u}_e = \mathbf{f}_e, \quad \mathbf{k}_e = \int_{\Omega^e} \mathbf{B}^T\mathbf{C}\mathbf{B}d\Omega = \int_{-1}^{+1}\int_{-1}^{+1} \mathbf{B}(\xi,\eta)^T\mathbf{C}\mathbf{B}(\xi,\eta)|J|\,d\xi d\eta \tag{25b}$$

The element contribution to $\mathbf{K}$ and $\mathbf{f}$ are as follows:

$$\mathbf{k}_{ij}^{e} = \begin{bmatrix} \mathbf{k}_{ij}^{uu} & \mathbf{k}_{ij}^{ua} & \mathbf{k}_{ij}^{ub} \\ \mathbf{k}_{ij}^{au} & \mathbf{k}_{ij}^{aa} & \mathbf{k}_{ij}^{ab} \\ \mathbf{k}_{ij}^{bu} & \mathbf{k}_{ij}^{ba} & \mathbf{k}_{ij}^{bb} \end{bmatrix} \tag{26a}$$

$$\mathbf{f}_i^e = \{\mathbf{f}_i^u \quad \mathbf{f}_i^a \quad \mathbf{f}_i^{b1} \quad \mathbf{f}_i^{b2} \quad \mathbf{f}_i^{b3} \quad \mathbf{f}_i^{b4} \quad \mathbf{f}_i^{b5} \quad \mathbf{f}_i^{b6} \quad \mathbf{f}_i^{b7} \quad \mathbf{f}_i^{b8}\}^T \tag{26b}$$

where the indices u, a and b refer, respectively, to the extended displacement vectors and the extended new (enriched) degrees of freedom vectors, so that

$$\mathbf{k}_{ij}^{rs} = \int_{\Omega_e} (\mathbf{B}_i^r)^T\mathbf{C}(\mathbf{B}_i^s)\,d\Omega \quad (r,s = u,a,b) \tag{27a}$$

$$\mathbf{f}_i^u = \int_{\partial\Omega_e} N_i\bar{t}d\Gamma + \int_{\Omega_e} N_i\mathbf{f}\,d\Omega \tag{27b}$$

$$\mathbf{f}_i^a = \int_{\partial\Omega_e} N_iH\bar{t}d\Gamma + \int_{\Omega_e} N_iH\mathbf{f}\,d\Omega \tag{27c}$$

$$\mathbf{f}_i^{b\alpha} = \int_{\partial\Omega_e} N_iF_\alpha\bar{t}d\Gamma + \int_{\Omega_e} N_iF_\alpha\mathbf{f}\,d\Omega \quad (\alpha = 1,8) \tag{27d}$$

In (27), $\mathbf{B}_i^u$, $\mathbf{B}_i^a$ and $\mathbf{B}_i^b$ are the matrices of shape function derivatives, which are defined as

$$\mathbf{B}_i = \begin{bmatrix} N_{i,x} & 0 & 0 & 0 \\ 0 & N_{i,y} & 0 & 0 \\ N_{i,y} & N_{i,x} & 0 & 0 \\ 0 & 0 & N_{i,x} & 0 \\ 0 & 0 & N_{i,y} & 0 \\ 0 & 0 & 0 & N_{i,x} \\ 0 & 0 & 0 & N_{i,y} \end{bmatrix} \tag{28a}$$

$$\mathbf{B}_i^a = \begin{bmatrix} (N_iH)_{,x} & 0 & 0 & 0 \\ 0 & (N_iH)_{,y} & 0 & 0 \\ (N_iH)_{,y} & (N_iH)_{,x} & 0 & 0 \\ 0 & 0 & (N_iH)_{,x} & 0 \\ 0 & 0 & (N_iH)_{,y} & 0 \\ 0 & 0 & 0 & (N_iH)_{,x} \\ 0 & 0 & 0 & (N_iH)_{,y} \end{bmatrix} \tag{28b}$$

$$\mathbf{B}_i^b = \begin{bmatrix} \mathbf{B}_i^{b1} & \mathbf{B}_i^{b2} & \mathbf{B}_i^{b3} & \mathbf{B}_i^{b4} & \mathbf{B}_i^{b5} & \mathbf{B}_i^{b6} & \mathbf{B}_i^{b7} & \mathbf{B}_i^{b8} \end{bmatrix} \tag{28c}$$

$$\mathbf{B}_i^{b\alpha} = \begin{bmatrix} (N_iF_\alpha)_{,x} & 0 & 0 & 0 \\ 0 & (N_iF_\alpha)_{,y} & 0 & 0 \\ (N_iF_\alpha)_{,y} & (N_iF_\alpha)_{,x} & 0 & 0 \\ 0 & 0 & (N_iF_\alpha)_{,x} & 0 \\ 0 & 0 & (N_iF_\alpha)_{,y} & 0 \\ 0 & 0 & 0 & (N_iF_\alpha)_{,x} \\ 0 & 0 & 0 & (N_iF_\alpha)_{,y} \end{bmatrix} \tag{28d}$$

5. ENRICHMENT FUNCTIONS

The asymptotic displacement fields in the vicinity of the the crack-tip in an unbounded MEE domain were derived in Section 3. From them, a set of elementary functions that span the asymptotic fields can be obtained for any orientation of the crack and loading combination. While for isotropic and piezoelectric materials, only four or six functions, respectively, are necessary to describe all the possible generalized displacement states near the crack tip, for MEE materials eight functions are needed. These functions, named as F_α in equation (21), are obtained from the asymptotic singular solution presented in Section 3, and can be expressed as an extension of those obtained in Reference [26] for piezoelectric materials to yield

$$F_\alpha(r,\theta) = \sqrt{r}\ \big\{\rho_1\cos(\theta_1/2) \quad \rho_2\cos(\theta_2/2) \quad \rho_3\cos(\theta_3/2)) \quad \rho_4\cos(\theta_4/2) \\ \rho_1\sin(\theta_1/2) \quad \rho_2\sin(\theta_2/2) \quad \rho_3\sin(\theta_3/2) \quad \rho_4\sin(\theta_4/2)\big\} \tag{29a}$$

where

$$\rho_K(\omega,\mu_K) = \frac{1}{\sqrt{2}}\sqrt[4]{2(|\mu_K|^2-1)(\sin\omega)^2 + \mathrm{Re}(\mu_K)\sin 2\omega - 1} \tag{29b}$$

and

$$\theta_K = \pi\mathrm{Int}(\frac{\omega}{\pi}) + \arctan\frac{|\mathrm{Im}(\mu_K)|\tan\left(\omega - \pi\mathrm{Int}(\frac{\omega}{\pi})\right)}{1+\mathrm{Re}(\mu_K)\tan\left(\omega-\pi\mathrm{Int}(\frac{\omega}{\pi})\right)}. \tag{29c}$$

In (29), $\omega = \theta - \alpha$ (Figure 1) and μ_I are the four roots of the characteristic equation whose imaginary part are positive.

A total of eight enrichment functions are thus obtained, as compared to the piezoelectric case where six were proposed [26] or the elastic case where only four were needed [23]. This is due to the fact that whereas in the elastic case only the modification of the mechanical fields induced by the presence of the crack needs to be described, in the piezoelectric and MEE cases

the crack also affects the electric field and the electric and magnetic fields, respectively. In the same way, the characteristic equation of the material (16) leads to eight roots μ_I in the MEE case, whereas the corresponding characteristic equations for piezoelectric and elastic materials lead to six and four roots, respectively.

6. COMPUTATION OF EXTENDED STRESS INTENSITY FACTORS

The mechanical stresses, electric displacements and magnetic inductions exhibit the classical $\sqrt{r}$ singular behavior near the crack tip [2, 10]. The amplitudes of such singular fields are characterized by the traditional stress intensity factors K_I and K_{II}, the electric displacemet intensity factor K_{IV}, and the magnetic induction intensity factor K_V. K_{IV} and K_V contain the information on the discontinuity induced by the crack into the electrical and magnetical fields, respectively. All these field intensity factors may be grouped together as an extended stress intensity factor (ESIF) vector:

$$\mathbf{K} = \begin{pmatrix} K_{II} \\ K_I \\ K_{IV} \\ K_V \end{pmatrix} \tag{30}$$

In this paper, the interaction integral technique developed by Rao and Kuna [34] for extraction of ESIFs in MEE materials is applied. A brief description of this approach follows. The path independent J-integral for a MEE cracked solid is given by [10, 11]

$$J = \int_\Gamma (W\delta_{1j} - \sigma_{ij}u_{i,1} - D_j\phi_{,1} - B_j\varphi_{,1})n_j \, d\Gamma \tag{31}$$

where the indexes i and j vary from 1 to 2 in a two-dimensional solid, Γ is an arbitrary enclosing contour around the crack tip and n_j is the j-th component of the outward unit vector normal

to it, and W is the electromagnetic enthalpy density, which for a linear MEE material can be expressed as

$$W = \frac{1}{2}(\sigma_{ij}\varepsilon_{ij} - D_j E_j - B_j H_j) \tag{32}$$

Equation (31) may be transformed into an equivalent domain expression by applying the divergence theorem:

$$J = \int_A (\sigma_{ij}u_{i,1} + D_j\phi_{,1} + B_j\varphi_{,1} - W\delta_{1j})q_{,j}\,dA + \int_A (\sigma_{ij}u_{i,1} + D_j\phi_{,1} + B_j\varphi_{,1} - W\delta_{1j})_{,j}q\,dA \tag{33}$$

where A is the area inside the contour Γ and q is an arbitrary smoothing function such that it is unity at the crack tip and zero on the boundary Γ. The second term in (33) vanishes in homogeneous MEE materials, yielding

$$J = \int_A (\sigma_{ij}u_{i,1} + D_j\phi_{,1} + B_j\varphi_{,1} - W\delta_{1j})q_{,j}\,dA. \tag{34}$$

Equations (32) and (34) can be rewritten in terms of the extended variables defined in (4) and (5) as

$$J = \int_A (\sigma_{Ij}u_{I,1} - W\delta_{1j})q_{,j}\,dA, \quad W = \frac{1}{2}\sigma_{Ij}\varepsilon_{Ij}. \tag{35}$$

Let us now consider two independent equilibrium states for the cracked body. The first one corresponding to the the state under study and the second one corresponding to an auxiliary state, which may be selected as the near-tip extended displacement field for any of the extended opening fracture modes. In this work, for the sake of convenience, the asymptotic fields are expressed in terms of the generalized Stroh's formalism [29, 35]. If a polar coordinates system (r, θ) with the origin at the crack tip is used, the extended displacement fields can be written as

$$u_I(r,\theta) = \sqrt{\frac{2}{\pi}}\mathrm{Re}\left(K_N A_{IM} B_{MN}^{-1}\sqrt{r\,(\cos\theta + \mu_M \sin\theta)}\right) \tag{36}$$

whereas the stresses fields can be expressed as

$$\sigma_{Ij}(r,\theta) = (-1)^j \sqrt{\frac{1}{2\pi}} \mathrm{Re}\left(K_N B_{IM} B^{-1}_{MN} \frac{\delta_{j1}\mu_M + \delta_{j2}}{\sqrt{r\left(\cos\theta + \mu_M \sin\theta\right)}} \right) \tag{37}$$

where the summation over N comprises all the fracture modes K_I, K_{II}, K_{IV} and K_V. In (36) and (37), the tensors $\mathbf{A}$ and $\mathbf{B}$, which depend on the materials properties, can be computed from the following eigenvalue problem:

$$\left(\begin{array}{c|c} -\mathbf{L}^{-1}\mathbf{M} & -\mathbf{L}^{-1} \\ \hline \mathbf{Z} - \mathbf{M}^T\mathbf{L}^{-1}\mathbf{M} & -\mathbf{M}^T\mathbf{L}^{-1} \end{array}\right) \left(\begin{array}{c} \mathbf{A}_M \\ \hline \mathbf{B}_M \end{array}\right) = \mu_M \left(\begin{array}{c} \mathbf{A}_M \\ \hline \mathbf{B}_M \end{array}\right) \quad \text{(no sum on M)} \tag{38}$$

with $\mathbf{L}$, $\mathbf{M}$ and $\mathbf{Z}$ being the tensors defined in Stroh's formalism as

$$\mathbf{Z} := \mathbf{C}_{1IJ1}, \quad \mathbf{M} := \mathbf{C}_{2IJ1}, \quad \mathbf{L} := \mathbf{C}_{2IJ2} \tag{39}$$

The superposition of these two states produces another equilibrium state for which the J-integral is

$$J^{(S)} = \int_A ((\sigma^1_{Ij} + \sigma^2_{Ij})(u^1_{I,1} + u^2_{I,1}) - W^S \delta_{1j}) q_{,j} dA, \quad W^{(S)} = \frac{1}{2}[(\sigma^{(1)}_{Ij} + \sigma^{(2)}_{Ij})(\varepsilon^{(1)}_{Ij} + \varepsilon^{(2)}_{Ij})] \tag{40}$$

The J-integral in (40) can be decomposed into

$$J^{(S)} = J^{(1)} + J^{(2)} + M^{(1,2)} \tag{41}$$

where M is the interaction integral, defined as

$$M^{(1,2)} = \int_A (\sigma^{(1)}_{Ij} u^{(2)}_{I,1} + \sigma^{(2)}_{Ij} u^{(1)}_{I,1} - W^{(1,2)} \delta_{1j}) q_{,j} dA \tag{42}$$

with

$$W^{(1,2)} = \frac{1}{2}(\sigma^{(1)}_{Ij} \varepsilon^{(2)}_{Ij} + \sigma^{(2)}_{Ij} \varepsilon^{(1)}_{Ij}) \tag{43}$$

The elecromagnetomechanical J-integral can be expressed in terms of the extended stress intensity factors as [34]

$$J = \frac{1}{2} K_M Y_{MN} K_N \tag{44}$$

where Y_{MN} is the (5×5) Irwin matrix, which depends on the material properties

$$Y_{MN} = \Re(i \cdot A_{M\alpha} B_{M\alpha}^{-1})$$

where $\mathbf{A}$ and $\mathbf{B}$ are defined in (38).

For two-dimensional problems, one can write for any equilibrium state

$$\begin{aligned} J = {} & \tfrac{1}{2}K_{II}^2 Y_{11} + \tfrac{1}{2}K_I^2 Y_{22} + \tfrac{1}{2}K_{IV}^2 Y_{44} + \tfrac{1}{2}K_V^2 Y_{55} + K_I K_{II} Y_{12} \\ & + K_I K_{IV} Y_{24} + K_I K_V Y_{25} + K_{II} K_{IV} Y_{14} + K_{II} K_V Y_{15} + K_{IV} K_V Y_{45} \end{aligned} \tag{45}$$

Substituting this expression into (41), the interaction integral can be rewritten as

$$\begin{aligned} M^{(1,2)} = {} & K_{II}^{(1)} K_{II}^{(2)} Y_{11} + K_I^{(1)} K_I^{(2)} Y_{22} + K_{IV}^{(1)} K_{IV}^{(2)} Y_{44} + K_V^{(1)} K_V^{(2)} Y_{55} \\ & + (K_I^{(1)} K_{II}^{(2)} + K_{II}^{(1)} K_I^{(2)}) Y_{12} + (K_I^{(1)} K_{IV}^{(2)} + K_{IV}^{(1)} K_I^{(2)}) Y_{24} + (K_I^{(1)} K_V^{(2)} + K_V^{(1)} K_I^{(2)}) Y_{25} \\ & + (K_{II}^{(1)} K_{IV}^{(2)} + K_{IV}^{(II)} K_I^{(2)}) Y_{14} + (K_{II}^{(1)} K_V^{(2)} + K_V^{(1)} K_{II}^{(2)}) Y_{15} + (K_{IV}^{(1)} K_V^{(2)} + K_V^{(II)} K_{IV}^{(2)}) Y_{45} \end{aligned} \tag{46}$$

The individual extended stress intensity factors are evaluated by solving the system of linear algebraic equations obtained from (46) by choosing appropriate auxiliary states. For instance, if auxiliary state is taken so that $K_I^{(2)} = 1$ and $K_{II}^{(2)} = 0$, $K_{IV}^{(2)} = 0$, $K_V^{(2)} = 0$, (46) can be reduced to

$$M^{(1,I)} = K_I^{(1)} Y_{22} + K_{II}^{(1)} Y_{12} + K_{IV}^{(1)} Y_{24} + K_V^{(1)} Y_{25} \tag{47}$$

Similarly, other three equations can be obtained as

$$M^{(1,II)} = K_I^{(1)} Y_{12} + K_{II}^{(1)} Y_{11} + K_{IV}^{(1)} Y_{14} + K_V^{(1)} Y_{15}$$

$$M^{(1,IV)} = K_I^{(1)} Y_{24} + K_{II}^{(1)} Y_{14} + K_{IV}^{(1)} Y_{44} + K_V^{(1)} Y_{45}$$

$$M^{(1,V)} = K_I^{(1)} Y_{25} + K_{II}^{(1)} Y_{15} + K_{IV}^{(1)} Y_{45} + K_V^{(1)} Y_{55}$$

Therefore, the determination of the extended stress intensity factors is reduced to solving

the following system of linear equations:

$$\begin{pmatrix} M^{(1,II)} \\ M^{(1,I)} \\ M^{(1,D)} \\ M^{(1,B)} \end{pmatrix} = \mathbf{Y} \begin{pmatrix} K_{II}^{(1)} \\ K_{I}^{(1)} \\ K_{IV}^{(1)} \\ K_{V}^{(1)} \end{pmatrix} \tag{48}$$

7. NUMERICAL EXAMPLES

Several static crack problems in MEE media are solved to validate the formulation. The first example corresponds to a Griffith crack in a MEE solid subjected to a combined far field magneto-electro-mechanical uniform loading. The exact solution for this problem was first reported by Gao et al. [2]. This analytical solution will be the basis to characterize the convergence of the newly derived MEE enrichment functions. Additional examples involving finite cracked domains are presented as well. In this case no analytical solutions are available in the literature and the numerical boundary element results previously presented by García-Sáchez et al. [13] will be adopted as the benchmark reference solution for comparison purposes. In Reference [13], this BE formulation yielded very accurate results—validation was done against analytical solutions for a Griffith crack and two interacting cracks under remote loading in an infinite MEE medium. In all the numerical simulations, a MEE composite material $BaTiO_3$–$CoFe_2O_4$ with a volume fraction $V_f = 0.5$ is considered. The material properties are listed in Table I.

Furthermore, a 2×2 Gauss quadrature rule is used in every non-enriched element, whereas for non-partitioned enriched elements a 5×5 Gauss rule is used. For enriched elements that are partitioned into subtriangles, a seven point Gauss rule is used in each subtriangle. Moreover,

Table I. Material properties of $BaTiO_3$–$CoFe_2O_4$ ($V_f = 0.5$).

c_{11} (GPa)	c_{12} (GPa)	c_{13} (GPa)	c_{33} (GPa)	c_{44}(GPa)
226	125	124	216	44
e_{31} (C/m^2)	e_{33} (C/m^2)	e_{15} (C/m^2)		
-2.2	9.3	5.8		
h_{31} (N/Am)	h_{33} (N/Am)	h_{15} (N/Am)		
290.2	350	275		
ϵ_{11} (C^2/Nm^2)	ϵ_{33} (C^2/Nm^2)			
56.4×10^{-10}	63.5×10^{-10}			
β_{11} (Ns/VC)	β_{33} (Ns/VC)			
5.367×10^{-12}	2737.5×10^{-12}			
γ_{11} (Ns^2/C^2)	γ_{33} (Ns^2/C^2)			
297×10^{-6}	83.5×10^{-6}			

linear quadrilateral elements are used in all numerical experiments.

7.1. Validation: Griffith crack

First, to validate the extended finite element implementation, a straight crack of length $2a$ parallel to the x_1 axis in an infinite domain is considered. The crack is subjected to a remote electromagnetomechanical load combination in the x_2 direction: σ_{22}^{∞}, D_2^{∞}, B_2^{∞}. The polarization direction of the material coincides with the x_2 axis (Figure 4).

Gao et al. [2] derived the exact analytical solution for this problem using a complex potential approach based on the extended version of Eshelby-Stroh's formalism [35]. Details of the

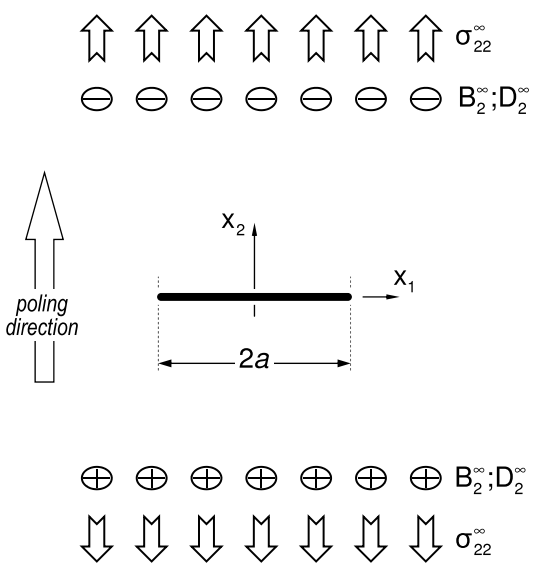

Figure 4. Griffith crack normal to the polarization direction of a MEE solid under remote loading.

procedure and the resulting field variables in the infinite cracked medium may be found in Reference [2]. The infinite solid is modeled using a finite square computational domain with a central crack. The resulting square plate width is $20a$ and it is loaded on its boundaries with the fields derived from the exact solution [2]. The finite element mesh consists of $N_e \times N_e$ uniform quadrilateral elements. The analytical solutions for the extended stress intensity factors (SIFs) for electromagnetic impermeable crack face boundary conditions are given by

$$K_I^* = \sigma_{22}^{\infty}\sqrt{\pi a}, \quad K_{II}^* = 0, \quad K_{IV}^* = D_2^{\infty}\sqrt{\pi a}, \quad K_V^* = B_2^{\infty}\sqrt{\pi a}. \tag{49}$$

Note that the exact values are independent of the material properties for the Griffith crack. The mode-I SIF K_I coincides with the well-known value for an isotropic materials and it depends only on the mechanical loading, being independent of the applied electric/magnetic loads. Similarly, the electric displacement intensity factor K_{IV} depends only on the applied electric load D_2^{∞}, whereas the magnetic induction intensity factor K_V depends only on the

applied magnetic load B_2^{∞}.

To obtain the X-FEM numerical results two enrichment strategies are adopted:

- The conventional X-FEM approach using a topological enrichment with the eight newly derived functions. In this case only the nodes belonging to elements enclosing the crack tip are enriched (Figure 3).
- A geometrical (fixed area) enrichment as proposed by Béchet et al. [36] and Laborde et al. [37] to improve the X-FEM accuracy. In this case the enrichment, with the eight functions derived, spans all nodes lying inside a circle of radius r_e centered at the crack tip (Figure 2). Two different radii are considered for the enriched domain: $r_e/a = 0.2$, 0.35.

Figures 6, 7 and 8 illustrate the convergence of the extended SIFs, by plotting in a log-log scale the relation between the mesh density and the error percentage for K_I, K_{IV} and K_V, respectively. In all cases geometrical enrichment performs quite better than topological enrichment and results for $r_e/a = 0.35$ are superior to those obtained for $r_e/a = 0.2$, as expected [36, 37]. Good agreement with the exact solution is observed and the behavior of the X-FEM results obtained for the MEE case is consistent with those previously observed in isotropic [36] and piezoelectric [26] materials.

7.2. Slanted central crack in a magnetoelectroelastic plate

A finite MEE plate with a central inclined crack under combined electro-magneto-mechanical loads is analyzed. In Figure 9, the geometry and loading, as well as one of the uniform meshes used for solving the problem are depicted. The ratio between the crack length and plate width is $a/w = 0.2$. The plate is under uniform tension in the x_2 direction σ_{22} and subjected to both electric and magnetic loadings: $D_2 = 10^{-10}\sigma_{22}$ CN^{-1} and $B_2 = 10^{-9}\sigma_{22}$ $\mathrm{A}^{-1}\mathrm{m}$. The

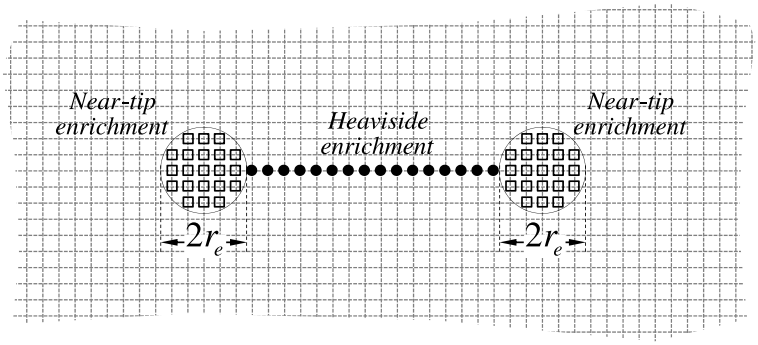

Figure 5. Geometrical enrichment strategy.

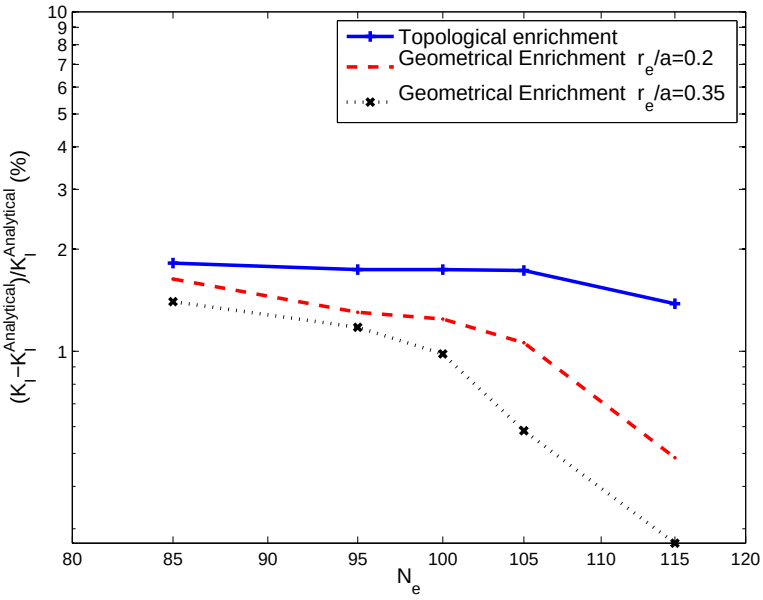

Figure 6. Mode-I SIF convergence for Griffith crack under remote magneto-electro-mechanical loading.

polarization direction coincides with the x_2 axis. The problem has been solved for two different uniform meshes (50×100, 75×150), and three different angles of the crack with respect to the x_1 axis ($\theta = 0°$, $15°$, $30°$). The extended finite element solutions are compared with those

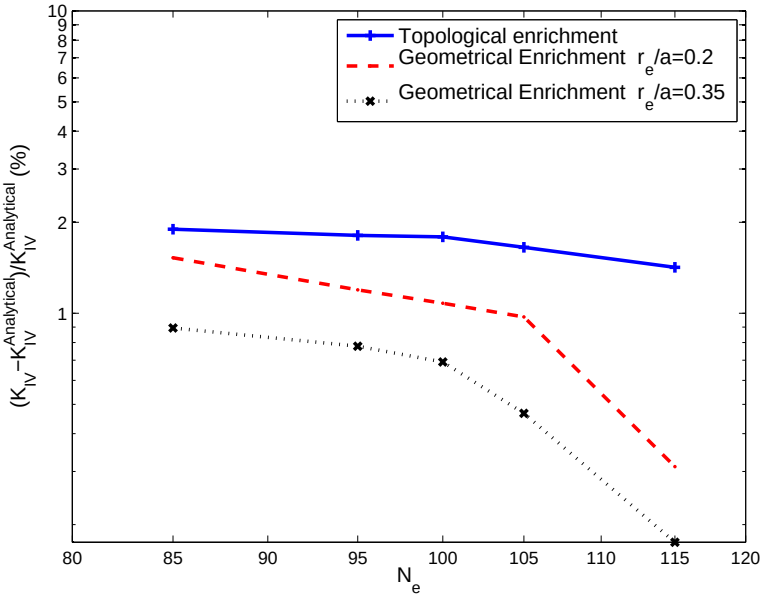

Figure 7. Electric displacement intensity factor convergence for Griffith crack under remote magneto-electro-mechanical loading.

obtained with the hypersingular BEM formulation developed by García-Sáchez et al. [13].

In Table II the reference BEM results are listed, and in Table III the normalized extended finite element results are presented for both topological enrichment and geometrical enrichment with $r_e/a = 0.35$. The extended SIFs obtained using the X-FEM are in good agreement with the BEM, with the geometrical enrichment strategy and the finer 75×150 mesh leading to results that are closer to the reference BEM solution.

7.3. Double-edge crack in magnetoelectroelastic plate

A double-edge crack in a finite MEE plate under combined electro-magneto-mechanical loads is analyzed. The geometry and loading, as well as one of the uniform meshes are illustrated

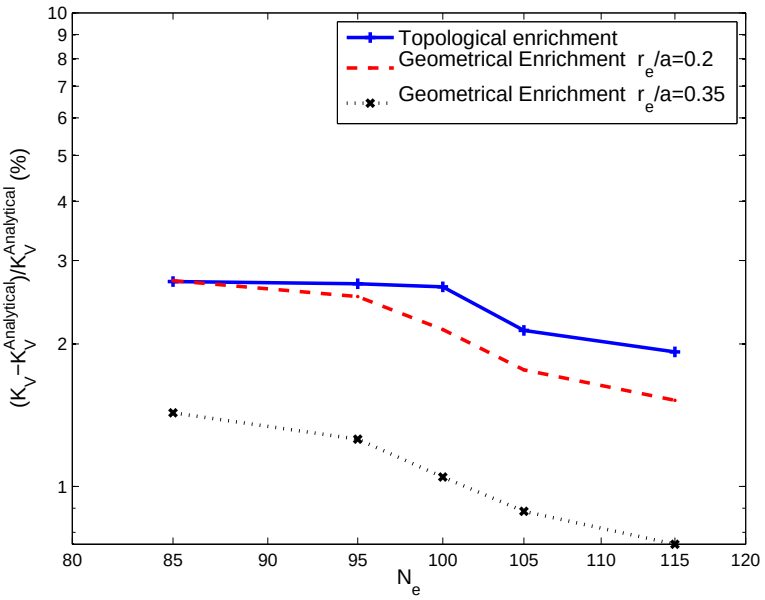

Figure 8. Magnetic induction intensity factor convergence for Griffith crack under remote magneto-electro-mechanical loading.

Table II. Reference boundary element SIFs for a slanted crack in a finite MEE plate.

θ	$\frac{K_I^{BEM}}{\sigma_{22}\sqrt{\pi a}}$	$\frac{K_{II}^{BEM}}{\sigma_{22}\sqrt{\pi a}}$	$\frac{K_{IV}^{BEM}}{D_2\sqrt{\pi a}}$	$\frac{K_V^{BEM}}{B_2\sqrt{\pi a}}$
0^o	1.0241	~ 0	1.0226	1.0395
15^o	0.9562	0.2506	0.9869	1.0103
30^o	0.7720	0.4361	0.8845	0.9206

in Figure 10. The ratio between the crack length and the plate width is given by $a/w = 0.25$. The load values and polarization angle are the same as in the previous example. Once again, the ESIFs obtained for two (50×100, 75×150) different uniform meshes with the X-FEM are in good agreement with the reference solution obtained by the dual BEM formulation [13]

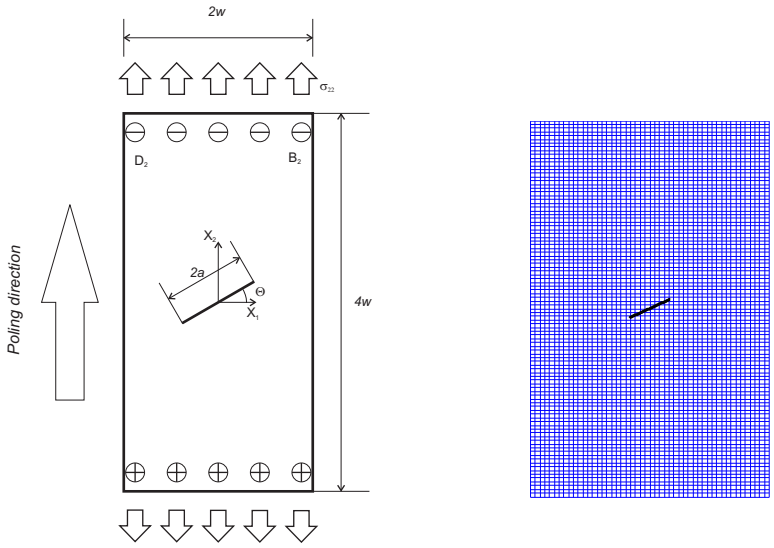

(a) (b)

Figure 9. Inclined crack in a rectangular MEE plate: (a) problem configuration; and (b) 50×100 mesh.

(see Tables IV and V). The X-FEM results are presented for topological enrichment as well as for geometrical enrichment with $r_e/a = 0.2$, 0.35. The latter enrichment strategy produces the more accurate result, with an error of less than 1 percent on the 75×150 mesh.

8. CONCLUDING REMARKS

An extended finite element method formulation for the analysis of fracture problems in bidimensional magnetoelectroelastic media was presented. New crack tip enrichment functions that represent the eight eigenfunctions of the asymptotic crack-tip expansion were obtained by extending the method proposed by Béchet et al. for piezoelectric solids [26] to MEE materials. The derivation of the domain form of the interaction integral to compute fracture parameters

Table III. Extended SIFs for slanted crack in a finite MEE plate.

θ	$ESIFs$	50×100 mesh topological enr.	50×100 mesh geometrical enr. ($r_e/a = 0.35$)	75×150 mesh topological enr.	75×150 mesh geometrical enr. ($r_e/a = 0.35$)
0^o	K_I/K_I^{BEM}	0.9911	1.0037	0.9916	1.0020
	K_{II}/K_{II}^{BEM}	-	-	-	-
	K_{IV}/K_{IV}^{BEM}	0.9940	1.0051	0.9952	1.0047
	K_V/K_V^{BEM}	0.9827	0.9894	0.9846	0.9941
15^o	K_I/K_I^{BEM}	0.9918	0.9984	0.9951	1.0008
	K_{II}/K_{II}^{BEM}	0.9885	1.0008	0.9876	0.9994
	K_{IV}/K_{IV}^{BEM}	1.0181	1.0161	1.0186	1.0162
	K_V/K_V^{BEM}	0.9575	0.9839	0.9723	0.9881
30^o	K_I/K_I^{BEM}	1.0062	1.0050	1.0116	1.0050
	K_{II}/K_{II}^{BEM}	1.0071	1.0067	0.9998	1.0006
	K_{IV}/K_{IV}^{BEM}	1.0178	1.0103	1.0137	1.0087
	K_V/K_V^{BEM}	0.9995	1.0083	0.9987	1.0013

Table IV. Reference boundary element extended SIFs for a double edge crack in a finite MEE plate.

$\frac{K_I^{BEM}}{\sigma_{22}\sqrt{\pi a}}$	$\frac{K_{II}^{BEM}}{\sigma_{22}\sqrt{\pi a}}$	$\frac{K_{IV}^{BEM}}{D_2\sqrt{\pi a}}$	$\frac{K_V^{BEM}}{B_2\sqrt{\pi a}}$
1.1197	-	1.1062	1.3636

was discussed in detail. The X-FEM results for several crack configurations were shown to be in excellent agreement with known analytical or numerical solutions [2, 13] for the stress,

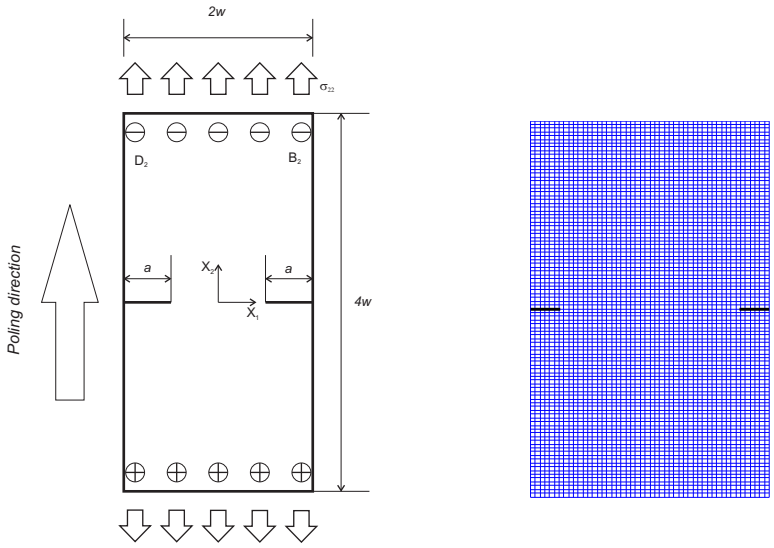

(a) (b)

Figure 10. Double-edge crack in a rectangular MEE plate: (a) problem configuration; and (b) 50×100 mesh.

electric displacement and magnetic induction intensity factors. Two enrichment strategies were adopted, namely a topological enrichment and a geometrical enrichment, where the latter was substantially better in terms of accuracy, which is consistent with studies for both isotropic [36, 37] and piezoelectric media [26].

Appendix A: Definition of the two-dimensional characteristics

The two dimensional material parameteres introduced in Section 3 follow from the three dimensional material properties defined in Section 2 as

$$a_{11} = \frac{1}{A}(c_{22}(\varepsilon_{22}\gamma_{22} - \alpha_{22}^2) + \varepsilon_{22}h_{22}^2 + \gamma_{22}e_{22}^2 - 2\alpha_{22}e_{22}h_{22})$$

Table V. Extended SIFs for a double edge crack in a MEE finite plate.

$ESIFs$	topological enr.	geometrical enr. ($r_e/a = 0.20$)	geometrical enr. ($r_e/a = 0.35$)
	50×100 mesh	50×100 mesh	50×100 mesh
K_I/K_I^{BEM}	0.9844	0.9850	0.9876
K_{IV}/K_{IV}^{BEM}	0.9885	0.9885	0.9890
K_V/K_V^{BEM}	0.9825	0.9915	0.9969
	75×150 mesh	75×150 mesh	75×150 mesh
K_I/K_I^{BEM}	0.9845	0.9862	0.9904
K_{IV}/K_{IV}^{BEM}	0.9848	0.9901	0.9934
K_V/K_V^{BEM}	0.9840	0.9938	1.0010

$$a_{12} = -\frac{1}{A}(c_{12}(\varepsilon_{22}\gamma_{22} - \alpha_{22}^2) + \varepsilon_{22}h_{21}h_{22} + \gamma_{22}e_{21}e_{22} - \alpha_{22}(e_{21}h_{22} - e_{22}h_{21}))$$

$$b_{21} = \frac{1}{A}(\gamma_{22}(c_{22}e_{21} - c_{12}e_{22}) - \alpha_{22}(c_{22}h_{21} - c_{12}h_{22}) + h_{22}(h_{22}e_{21} - h_{21}e_{22}))$$

$$d_{21} = -\frac{1}{A}(\varepsilon_{22}(c_{12}h_{22} - c_{22}h_{21}) + \alpha_{22}(c_{22}e_{21} - c_{12}e_{22}) + e_{22}(h_{22}e_{21} - h_{21}e_{22}))$$

$$a_{22} = \frac{1}{A}(\gamma_{22}(c_{11}\varepsilon_{22} + e_{21}^2) + \varepsilon_{22}h_{21}^2 - \alpha_{22}(c_{11}\alpha_{22} + 2e_{21}h_{21}))$$

$$b_{22} = -\frac{1}{A}(\gamma_{22}(c_{12}e_{21} - c_{11}e_{22}) - \alpha_{22}(c_{12}h_{21} - c_{11}h_{22}) + h_{21}(h_{22}e_{21} - h_{21}e_{22}))$$

$$d_{22} = \frac{1}{A}(\varepsilon_{22}(c_{11}h_{22} - c_{12}h_{21}) + \alpha_{22}(c_{12}e_{21} - c_{11}e_{22}) + e_{21}(h_{22}e_{21} - h_{21}e_{22}))$$

$$a_{33} = \frac{1}{B}(\gamma_{11}\varepsilon_{11} - \alpha_{11}^2)$$

$$b_{13} = \frac{1}{B}(\gamma_{11}e_{13} - h_{13}\alpha_{11})$$

$$d_{13} = -\frac{1}{B}(\alpha_{11}e_{13} - h_{13}\varepsilon_{11})$$

$$\delta_{11} = \frac{1}{B}(\gamma_{11}c_{33} + h_{13}^2)$$

$$\Delta_{11} = -\frac{1}{B}(\alpha_{11}c_{33} + e_{13}h_{13})$$

$$\delta_{22} = \frac{1}{A}(\gamma_{22}(c_{11}c_{22} - c_{12}^2) + c_{11}h_{22}^2 + c_{22}h_{21}^2 - 2c_{12}h_{12}h_{22})$$

$$\Delta_{22} = -\frac{1}{A}(\alpha_{22}(c_{11}c_{22} - c_{12}^2) + c_{11}e_{22}h_{22} + c_{22}e_{21}h_{21} - c_{12}(e_{22}h_{21} + e_{21}h_{22}))$$

$$\zeta_{11} = \frac{1}{B}(\varepsilon_{11}c_{33} + e_{13}^2)$$

$$\zeta_{22} = \frac{1}{A}(\varepsilon_{22}(c_{11}c_{22} - c_{12}^2) + c_{11}e_{22}^2 + c_{22}e_{21}^2 - 2c_{12}e_{12}e_{22})$$

where the Voigt notation has been used and

$$A = (c_{11}c_{22} - c_{12}^2)(\varepsilon_{22}\gamma 22 - \alpha_{22}^2) + e_{21}^2(c_{22}\gamma 22 + h_{22}^2) + e_{22}^2(c_{11}\gamma 22 + h_{21}^2)$$
$$+2\alpha_{22}(e_{21}(c_{12}h_{22} - c_{22}h_{21}) + e_{22}(c_{12}h_{21} - c_{11}h_{22})) - 2e_{21}e_{22}(c_{12}\gamma_{22} + h_{21}h_{22})$$
$$+\varepsilon_{22}(c_{11}h_{22}^2 + c_{22}h_{21}^2 - c_{12}h_{21}h_{22})$$

and

$$B = \varepsilon_{11}(c_{33}\gamma_{11} + h13^2) - \alpha_{11}(c_{33}\alpha_{11} + 2e_{13}h_{13}) + \gamma_{11}e_{13}^2$$

REFERENCES

1. C.-W. Nan, M. I. Bichurin, S. Dong, D. Viehland, and G. Srinivasan, Multiferroic magnetoelectric composites: Historical perspective, status, and future directions, Journal of Applied Physics, **103**(3):031101, 2008.
2. C.F. Gao, H. Kessler, and H. Balke, Crack problems in magnetoelectroelastic solids. Part I: exact solution of a crack, International Journal of Enginering Science, **41**:969–981, 2003.
3. C. F. Gao, H. Kessler, and H. Balke, Crack problems in magnetoelectroelastic solids. Part II: General solution of collinear cracks, International Journal of Enginering Science, **41**:983–994, 2003.
4. C. F. Gao, P. Tong, and T. Y. Zhang, Interfacial crack problems in magneto-electroelastic solids, International Journal of Enginering Science, **41**:2105–2121, 2003.

5. C. F. Gao, P. Tong, and T. Y. Zhang, Fracture mechanics for a mode III crack in a magnetoelectroelastic solid, International Journal of Solids and Structures, **41**:6613–6629, 2004.
6. G. C. Sih and Z. F. Song, Magnetic and electric poling effects associated with crack growth in $BaTiO_3$–$CoFe_2O_4$ composite, Theoretical and Applied Fracture Mechanics, **39**:209–227, 2003.
7. G. C. Sih and Z. F. Song, Piezomagnetic and piezoelectric poling effects on mode I and II crack initiation behaviour of magnetoelectroelastic materials composite, Theoretical and Applied Fracture Mechanics, **40**:161–186, 2003.
8. G. C. Sih and H. Y. Yu, Volume fraction effect of magnetoelectroelastic composite on enhancement and impediment of crack growth, Composite structures, **68**:1–11, 2005.
9. Z. F. Song and G. C. Sih, Crack initiation behavior in magnetoelectroelastic composite under in-plane deformation, Theoretical and Applied Fracture Mechanics, **39**:189–207, 2003.
10. B. L. Wang and Y. W. Mai, Crack tip field in piezoelectric/piezomagnetic media, European Journal of Mechanics - A/Solids, **22**:591–602, 2003.
11. B. L. Wang and Y. W. Mai, Fracture of piezoelectromagnetic materials, Mechanics Research Communications, **31**: 65–73, 2004.
12. W. Y. Tian and R. K. N. D. Rajapakse, Fracture analysis of magnetoelectroelastic solids by using path independent integrals, International Journal of Fracture, **131**:311–335, 2005.
13. F. García-Sánchez, R. Rojas-Díaz, A. Sáez, and Ch. Zhang, Fracture of magnetoelectroelastic composite materials using boundary element method (BEM), Theoretical and Applied Fracture Mechanics, **47**(3):192–204, 2007.
14. J. Sladek, V. Sladek, P. Solek, and E. Pan, Fracture analysis of cracks in magneto-electro-elastic solids by the MLPG, Computational Mechanics, **42**:697–714, 2008.
15. G. R. Buchanan, H. Kessler, and H. Balke, Layered versus multiphase magneto-electro-elastic composites, Composites Part B: Engineering, **35**(5):413–420, 2004.
16. R. M. Garcia Lage, C. M. Mota Soares, and C. A. Mota Soares, Layerwise partial mixed finite element analysis of magneto-electro-elastic plates, Computers and Structures, **82**: 1293–1301, 2004.
17. R. K. Bhangale and N. Ganesan, Static analysis of simply supported functionally graded and layered magneto-electro-elastic plates, **43**:3230–3253, 2006.
18. R. K. Bhangale and N. Ganesan, Free vibration of simply supported functionally graded and layered magneto-electro-elastic plates by finite element method, Journal of Sound and Vibration, **294**:1016–1038, 2006.

19. A. R. Annigeri, N. Ganesan, and S. Swarnamani, Free vibrations of clamped-clamped magneto-electro-elastic cylindrical shells, Journal of Sound and Vibration, **292**:300–314, 2006.

20. A. Daga, N. Ganesan, and K. Shankar, Behaviour of magneto-electro-elastic sensors under transient mechanical loading, Sensors and Actuators A: Physical, **150**:46–55, 2009.

21. J. M. Simoes Moita, C. M. Mota Soares, and C. A. Mota Soares, Analyses of magneto-electro-elastic plates using a higher order finite element model, Composite Structures, **91**:421–426, 2009.

22. B. Wang and Y. W. Mai, Self-consistent analysis of coupled magnetoelectroelastic fracture. Theoretical investigation and finite element verigfication, Computer Methods in Applied Mechanics and Engineering, **196**:2044-2054, 2007.

23. N. Moës, J. Dolbow, and T. Belytschko. A finite element method for crack growth without remeshing, International Journal for Numerical Methods in Engineering, **46**:131-150, 1999.

24. N. Sukumar, Z. Y. Huang, J.-H. Prvost, and Z. Suo, Partition of unity enrichment for bimaterial interface cracks, International Journal for Numerical Methods in Engineering, **59**:1075–1102, 2004

25. A. Asadpoure and S. Mohammadi. Developing new enrichment functions for crack simulation in orthotropic media by the extended finite element method. International Journal for Numerical Methods in Engineering, **69**:2150-2172, 2007.

26. E. Béchet, M. Scherzer, and M. Kuna, Application of the X-FEM to the fracture of piezoelectric materials, International Journal for Numerical Methods in Engineering, **77**:1535–1565, 2009.

27. T. P. Fries and T. Belytschko, The extended/generalized finite element method: An overview of the method and its applications, International Journal for Numerical Methods in Engineering, 2010. DOI: 10.1002/nme.2914.

28. A. K. Soh and J. X. Liu, On the Constitutive Equations of Magnetoelectroelastic Solids, Journal of Intelligent Material Systems and Structures, **16**: 597–602, 2005.

29. D. M. Barnett and J. Lothe, 1975 Dislocations and Line Charges in Anisotropic Piezoelectric Insulators, Phys. Stat. Sol., **67(b)**:105–111, 1975.

30. W. Y. Tian and R. K. N. D. Rajapakse, Theoretical modelling of a conducting crack in a magnetoelectroelastic solid, International Journal of Applied Electromagnetics and Mechanics, **22**:141–158, 2005.

31. H. Sosa, Plane problems in piezoelectric media with defects, International Journal of Solids and Structures, **28**:491–505, 1991.

32. T. Belytschko and T. Black, Elastic crack growth in finite elements with minimal remeshing, International

Journal for Numerical Methods in Engineering, **45**:601-620, 1999.

33. I. Babuška and J. M. Melenk. The partition of unity method. International Journal for Numerical Methods in Engineering, **4**:607–632, 1997.
34. B. N. Rao and M. Kuna, Interaction integrals for fracture analysis of functionally graded magnetoelectroelastic materials, International Journal of Fracture, **153**:15–37, 2008.
35. A. N. Stroh, Dislocations and cracks in anisotropic elasticity, Philos. Mag., **3**:625–646, 1958.
36. E. Béchet, H. Minnebo, N. Moës, and B. Burgardt, Improved implementation and robustness study of the X-FEM for stress analysis around cracks, International Journal for Numerical Methods in Engineering, **64**:1033–1056, 2005.
37. P. Laborde, J. Pommier, Y. Renard, and M. Salan, High-order extended finite element method for cracked domains, International Journal for Numerical Methods in Engineering, **64**:354-381, 2005.

